Continental Shelf Research 268 (2023) 105116

Contents lists available at ScienceDirect

Continental Shelf Research

journal homepage: www.elsevier.com/locate/csr

Sediment-water fluxes of inorganic carbon and nutrients in the Pacific Arctic during the sea ice melt season

Lauren J. Barrett [a,*], Penny Vlahos [a], Douglas E. Hammond [b], Robert P. Mason [a]

[a] Department of Marine Sciences, University of Connecticut, 1080 Shennecossett Rd, Groton, CT, 06340, USA
[b] Department of Earth Sciences, University of Southern California, 3651 Trousdale Pkwy, Los Angeles, CA, 90089, USA

ARTICLE INFO

Keywords:
Sediment
Arctic
Benthic flux
Carbon cycle
Inorganic carbon
Biogeochemistry

ABSTRACT

The Bering and Chukchi Seas are important oceanic regions of carbon dioxide (CO_2) uptake owing to enhanced gas solubility in cold surface waters and highly productive spring phytoplankton blooms. Over the past several decades, sea ice extent in the Arctic Ocean has decreased and the ice-melt season has started earlier in the year, but the biogeochemical impacts of these systematic changes are unclear. As these marginal seas of the Arctic Ocean are quite shallow (mostly <60 m depth) there is extensive interaction across air-sea-sediment boundaries, and export production rates are high during the spring bloom, delivering organic carbon to the sediments. However, the subsequent transformations and fluxes of carbon in Bering and Chukchi Sea sediments have not been directly quantified. In May–June 2021, we collected sediment cores at 5 stations spanning the eastern Bering Sea and southern and eastern Chukchi Sea. These stations encompassed a range of surface water ice coverage history, from greater than one month to less than one day of ice-free conditions. In the Chukchi Sea, dissolved nutrient and inorganic carbon (DIC) effluxes from the sediments decreased northward. The highest and most variable DIC fluxes were observed in the southern Chukchi Sea, north of the Bering Strait, ranging from 2.0 to 21.5 mmol m^{-2} d^{-1}, while the lowest DIC fluxes were observed at the northernmost Chukchi Sea station near Cape Lisburne, ranging from 1.1 to 2.3 mmol m^{-2} d^{-1}. Moving northward, the surface water had greater sea ice concentrations, inhibiting surface productivity and air-sea exchange of CO_2. The reduced export of labile carbon to the seafloor likely resulted in decreased benthic respiration and thus a lower flux of remineralization products from the sediments to the water column. Some duplicate core measurements were highly heterogeneous, especially in the Bering Sea, illustrating the dynamic nature of this macrofauna-dominated benthic environment and the range of fluxes under different rates of infaunal activity. Core replicates with relatively higher effluxes of remineralization products also had high fluxes of radon-222, a proxy for bio-irrigation in sediments, illustrating the dominant role of benthic macrofauna in benthic-pelagic coupling in this region. While these observations serve as a seasonal reference, they may also demonstrate how sedimentary fluxes will evolve under future conditions wherein sea ice retreats earlier in the season.

1. Introduction

The Arctic Ocean is a significant sink for atmospheric carbon dioxide (CO_2). Although it represents less than 5% of global sea surface area, it accounts for up to 12% of global sea surface carbon uptake (Yasunaka et al., 2018). Myriad processes influence carbon cycling in the Arctic Ocean and its marginal seas, including air-sea exchange, temperature and salinity, ice coverage, freshwater input, water mass circulation, and primary productivity (Cai et al., 2010). The relative contributions of these factors are changing as the Arctic undergoes rapid climate change. Over the past several decades, the maximum extent of sea ice in the Arctic Ocean has decreased (Wang and Overland, 2009), and the melt-season has lengthened by about 5 days per decade, with both an earlier melt onset and later freeze-up time (Stroeve et al., 2014). Sea ice coverage has a strong influence on Arctic Ocean circulation patterns and thus on the transport of nutrients and carbon, and the future changes to the carbon cycle resulting from this systematic change to ice characteristics are unclear.

The efficiency of carbon uptake in the Arctic Ocean is attributed to the enhanced solubility of CO_2 in cold, fresh water as well as the large

* Corresponding author.
E-mail address: lauren.jo.barrett@gmail.com (L.J. Barrett).

https://doi.org/10.1016/j.csr.2023.105116
Received 7 April 2023; Received in revised form 6 September 2023; Accepted 8 September 2023
Available online 9 September 2023

atmosphere-ocean pCO_2 gradient caused by high summertime productivity and the export of carbon to sediments (Omar et al., 2007). Some researchers predict that the rate of carbon uptake in this region will increase as sea ice melt exposes greater surface water area (Bates, 2006). However, others posit that the efficiency of CO_2 uptake in the Arctic will not change appreciably in the future; for example, the freshening of the Arctic can also act to negate CO_2 uptake as the buffering capacity is diluted and enhanced stratification blocks carbon sequestration in deeper waters (Cai et al., 2010; Woosley and Millero, 2020; DeGrandpre et al., 2020). Increased zooplankton grazing under warmer conditions could also decrease carbon export to sediments (Wang et al., 2019). The heterogeneous nature of sea ice coverage, freshwater input, and water mass circulation in the Arctic Ocean and its adjacent seas also complicates this analysis. Some authors predict that the net annual Chukchi Sea CO_2 sink is decreasing based on remotely sensed chlorophyll-a concentrations (Yasunaka et al., 2018) and direct pCO_2 measurements (Wang et al., 2021), while others predict that the CO_2 sink is increasing due to enhanced primary productivity (Ouyang et al., 2020).

The Bering and Chukchi Seas are of particular interest in understanding Arctic Ocean biogeochemical cycles and carbon sequestration because this region is the only gateway for nutrient and CO_2-rich Pacific-sourced waters to enter the Arctic Ocean (Coachman et al., 1981). The transport of nutrient-replete Pacific waters to the euphotic zone of the northern Bering and Chukchi Seas fuels high rates of primary productivity, stimulated in the spring by receding sea ice and increasing day length. As such, the Chukchi Sea is one of the most productive Arctic marginal seas (Arrigo and van Dijken, 2011) and the vertical export of carbon is critical to carbon sequestration in this area (MacGilchrist et al., 2014). However, the future fate of primary productivity and the biological pump in these seas is uncertain due to the earlier seasonal onset of sea ice retreat and the increasing transport of Pacific waters through the Bering Strait (Woodgate, 2018). Some authors have shown increased primary productivity due to a longer open-water season and the presence of melt ponds that increase light penetration, enhancing under-ice blooms (Arrigo et al., 2012), while others hypothesize that early spring nitrate exhaustion reduces the overall carbon uptake in the Chukchi Sea (Kwon et al., 2022). The Bering and Chukchi Seas are shallow (<60 m) and therefore interact extensively with the sediments, which may also impact carbon cycling and long-term storage.

The seasonal cycles of sea ice and productivity in the Arctic also influence the cycling of nutrients in this region. The storage and transformation of nutrients and carbon in sediments can impact their surface water distribution, especially in shallow shelf regions with substantial benthic-pelagic coupling such as the marginal seas of the Arctic Ocean (Dunton et al., 2005). Studies of biomass and macrofaunal distribution in western Arctic sediments have shown that this region is dominated by perennial infauna including amphipods and bivalves (Grebmeier, 1987, 1989) and that water mass dynamics strongly influence sedimentary carbon deposition (Grebmeier et al., 1995). More recent work has shown that the region just north of the Bering Strait is a benthic macrofauna biomass "hotspot" with concentrations up to 25 g C m^{-2} (Grebmeier et al., 2015). This results in part from the incomplete consumption of primary producers by zooplankton in the region, leading to high rates of export production (Campbell et al., 2009) and benthic control of upper trophic levels (Grebmeier, 2012). While the delivery of organic carbon to sediments is well-characterized in the Bering and Chukchi Seas, there is relatively little information about the subsequent transformation of this material and the efflux of inorganic carbon, which could have important impacts on carbon cycling and sequestration. Sediment-water CO_2 fluxes have been indirectly estimated for this area via sediment oxygen demand (SOD, Moran et al., 2005; Grebmeier, 2012). Based on these estimates, Moran et al. (2005) showed a two-fold increase in benthic carbon respiration between May and July of 2002 on the Chukchi Sea shelf. This increase was attributed to increased export production, as particulate organic carbon (POC) flux increased about fourfold in the same time period. Due to increased water column grazing, POC export and benthic respiration were decoupled as the summer progressed. While this previous work provides foundational estimates of benthic inorganic carbon content, to date there have been no direct quantifications of the contribution of sediments to CO_2 cycling in this region. The climate change-driven transformations in sea ice coverage, primary production, and water mass transport further motivate the investigation of benthic fluxes of inorganic carbon, especially with regards to regional acidification, which has already been observed in the Bering (Sun et al., 2021) and Chukchi Seas (Yamamoto-Kawai et al., 2016). A holistic understanding of biogeochemical cycling in this region is important for predicting future carbon uptake in a changing climate as well as downstream effects on the Arctic Ocean basin.

Here we quantify fluxes of dissolved inorganic carbon (DIC), total alkalinity (TA), and nutrients (nitrate, ammonium, silicic acid, and phosphate) at the sediment-water interface at five locations in the Bering and Chukchi Seas (Fig. 1). Fluxes of radon-222 (^{222}Rn) were also measured as an indicator of non-diffusive transport facilitated by infaunal irrigation. These fluxes were measured in late spring (May–June 2021) and span a range of ice coverage conditions. The results are used to discern the indirect effects of ice coverage on sediment-water interactions and are compared to the overlying water column conditions and to previous flux estimates.

2. Methods

2.1. Water column sample collection

Discrete water column samples were collected at 14 stations onboard the *R/V Sikuliaq* from May 20 to June 14, 2021. Samples in open seawater were collected into 30 L Niskin bottles before subsampling. DIC samples were collected into 20 mL borosilicate vials with aluminum crimp lids and PTFE septa and were preserved with saturated mercuric chloride to a final concentration of 0.05% v/v. Nutrient samples (N, P)

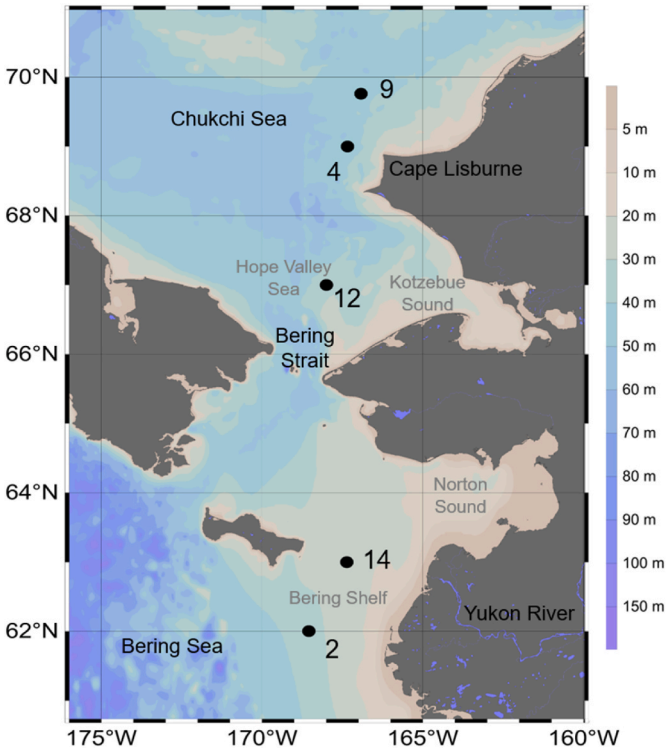

Fig. 1. Sediment core locations with station and regional identifiers from cruise SKQ2021-08 S. Bathymetry shown by the color scale is from the etopo1 dataset (Armante and Eakins, 2009). The map was generated using Ocean Data View version 5.6.3 (2022).

were filtered through glass fiber filters (GFF, nominal pore size 0.7 μm) into 20 mL HDPE vials and frozen to < -20 °C. Salinity samples were collected into 250 mL glass bottles and analyzed within 2 days on a shipboard Portasal salinometer. Samples for pH were collected directly from 30 L Niskin bottles into 10 cm pathlength stoppered quartz cuvettes (~35 mL volume), allowing at least one volume overflow to extrude bubbles.

2.2. Sediment cores and incubation sampling

A multi-corer was used to collect replicate gravity cores (9.5 cm ID) at 5 stations (Fig. 1). Two of these, with undisturbed sediment-water interfaces, were selected for core incubations. Immediately after multicore retrieval, each core was plugged at its base and a piston with a tube allowing water through-flow was inserted in the tube top, taking care to avoid trapping bubbles. The piston was advanced to a position where about 15 cm of coretop water remained (~1 L water volume), and the incubation began. Incubations were carried out in a dark cold room (~3 °C) for 1 week using the methodology of Hammond et al. (2004). Briefly, the sampling piston was advanced as water aliquots were periodically removed for analysis. For each interval, time divided by water column height was computed and concentrations were plotted against the sum of this parameter. If flux is constant, this relationship should be linear, and flux can be calculated from a linear regression to the observed data. A stirring bar housed just below the piston was rotated continuously at ~40 rpm, which kept the overlying water well-mixed and should limit the boundary layer thickness of water just above the sediment-water interface to about 100 μm (Hammond et al., 2004). Porewater profiles of the analytes measured are expected to have significantly longer length scales, so stirring rate is not expected to strongly affect the measured fluxes. Temperature (3–4 °C) was monitored during the incubation, and a small correction was made to adjust fluxes to in situ temperature. Samples were drawn at various times for DIC, pH, nutrients, and ^{222}Rn. Water remaining at the conclusion of the experiment was used for analysis of radium isotopes (223, 224 and 228); these results will be discussed elsewhere. After the incubation experiments were completed, one replicate sediment core was sectioned into 1 cm segments. During sectioning, it was clear that sediments contained abundant worms, sand dollars, gastropods, clams, shrimp-like creatures, and some burrows extending as deep as ~22 cm. Incubation core 2 A captured a cnidarian that emerged about 7 cm from its burrow during the incubation (Fig. S1), explaining the very large solute flux observed in this core relative to its replicate (2 B). At some stations, active irrigation was evident by the presence of mineralized tube structures with rusty coatings, at depths up to 22 cm. Cores were a lighter color near the surface, likely a more oxidized region, with a few exhibiting black pockets at depth, likely reflecting the presence of iron sulfides.

2.3. Analytical measurements

DIC, pH, and nutrients were sampled from the overlying water in the incubation apparatus at multiple time-points throughout the incubation. For sediment flux incubations, DIC samples were collected into the same vial type and preserved using the same method as the water column samples. DIC was analyzed in the laboratory within six months of collection using a Shimadzu TOC-L Analyzer (USGS, 2019) calibrated with CO_2 CRMs with an average run precision of ±4.5 μmol kg^{-1} or 0.2%.

Sample pH was analyzed at 25 °C within ~1 h of collection using an Agilent Cary60 UV/Vis spectrophotometer and m-cresol purple indicator dye, following Dickson et al. (2007). The dye solution was prepared to a concentration of 2.05 mM, amended with aqueous NaOH to a pH of 8.03, and stored in a 20 mL HDPE container covered with foil and in the dark. The m-cresol purple dye was not purified, and this can lead to errors on the order of 0.005–0.01 pH units (Douglas and Byrne, 2017), which has been accounted for in data presentation and error propagation. The sample cells were brought to 25 °C in a water bath for at least 30 min, after which blank absorbance readings were taken. 50 μL of m-cresol purple dye solution was then added to the sample before measuring the absorbance again at 730, 578, and 434 nm. The final pH at 25 °C was calculated as described in Clayton and Byrne (1993). In-situ pH_T was later calculated using DIC, salinity, and temperature in CO2SYS (Humphreys et al., 2022).

Salinity was measured within 2 days of sample collection using a shipboard Portasal Salinometer 8410 A. Salinity samples were calibrated against IAPSO standard seawater, and the average sample precision was 0.006. The salinity results presented here are unitless practical salinity values, following TEOS-10.

Time-series overlying water samples were analyzed at UConn for ammonium (NH_4^+), phosphate (PO_4^{3-}), nitrate (NO_3^-), and nitrite (NO_2^-) using a SmartChem 200 discrete auto-analyzer. Nitrate was measured following SM 4500-NO_3-E (APHA, 2011) and EPA 353.2, Rev. 2 (EPA, 1993) using Cd reduction and calibrated against standard solutions ranging from 0 to 20 μM in artificial seawater (LOD 0.47 μM, replicate precision 0.16 μM, sample precision 0.59 μM). Nitrite was measured following SM 4500-NO2-B (APHA, 2013) and EPA 353.2 (EPA, 1993) and calibrated against standard solutions ranging from 0 to 20 μM in artificial seawater (LOD 0.44 μM, replicate precision 0.18 μM, sample precision 0.03 μM). Ammonium was measured following SM-4500-NH_3 F (APHA, 1997) and calibrated against standard solutions ranging from 0 to 20 μM in filtered aged seawater (LOD 0.92 μM, replicate precision 0.14 μM, sample precision 0.36 μM). Phosphate was measured following SM 4500-P-E (APHA, 1999) and calibrated against standards ranging from 0 to 10.5 μM in MilliQ water (LOD 0.46 μM, replicate precision 0.02 μM, sample precision 0.08 μM). Core incubation samples for silicate were filtered through polyether sulfone (PES) filters and refrigerated until analysis using the colorimetric methodology of Parsons et al. (1984) with a precision of ±3% or ±1 μM, whichever is larger.

Rn-222 was measured by drawing about 60 mL of overlying water from the incubation cell into a syringe, using a vacuum extraction technique to transfer it into a Lucas Cell, and counting the cell with an Applied Techniques counter (Berelson et al., 1987). Equations for calculating fluxes of a short-lived radionuclide using a core incubation can be found in Kemnitz and Hammond (2022). Initial core-top water concentration was assumed to be equal to bottom water collected from Niskin bottles at each station, an assumption validated by the similarity of initial core-top water nutrient concentrations to bottom water samples.

2.4. Computation

TA and the saturation state of aragonite (Ω_{arag}) were calculated from DIC, pH_T, salinity, temperature, phosphate, and silicate using the PyCO2SYS Python package (Humphreys et al., 2022). The empirical constants used in these calculations were those of Lueker et al. (2000), Dickson and Riley (1979), Dickson (1990), and Lee et al. (2010).

Sediment-water fluxes were calculated by the approach of Hammond et al. (2004), using the slope of a linear regression of concentration versus the integrated ratio of time/height in each core (Fig. S2). To best approximate in-situ conditions, only time points within the first 3.5 days of incubation were included in the flux calculation. This method minimized long-term incubation artifacts appearing as infauna became oxygen-stressed and increased irrigation rates. Though oxygen was not directly measured, a notable shift in inorganic nitrogen speciation from nitrate to ammonium consistently occurred after three days, indicating a transition to low-oxygen conditions. Elevated irrigation rates, likely due to oxygen stress to infaunal organisms, were also evident in the silicic acid fluxes that sometimes increased dramatically after ~3 days. Flux uncertainties are reported as either the standard error of the linear regression or the propagated regression error from analytical uncertainty, whichever is larger.

3. Results & discussion

3.1. In-situ conditions

The initial biogeochemical conditions of the overlying water for each incubated sediment core are summarized in Table 1. Stations are ordered from south to north reading from the top to bottom of table. All stations have a water column depth <50 m (see Fig. 1). Stations 2 and 14 are in the Bering Sea near the mouth of the Yukon River, which discharges ~200 km^3 yr^{-1} freshwater to the northern Bering Sea, with peak discharge rates in June (Yang et al., 2009). Station 14 is more influenced at the surface by freshwater inputs than station 2. Accordingly, higher sea surface temperature (SST) and lower sea surface salinity (SSS) were observed at station 14 than at station 2 (SSS = 24.7 and 30, SST = 5.0 and −0.57 °C for stations 14 and 2, respectively). Due to the spring freshet, the Yukon River discharge rate rapidly increased from less than 100,000 cfs (~2800 m^3/s) at the beginning of May 2021 to greater than 500,000 cfs (~14000 m^3/s) in the weeks leading up to our sampling period. Station 2 was sampled early in the study period on 23 May, while station 14 was sampled several weeks later, on 6 June.

The remaining three stations were in the Chukchi Sea. Station 12 is in the southern Chukchi Sea (Hope Sea Valley) and is influenced by the summertime flow of Bering Shelf-Anadyr Water (BSAW) which is nutrient-rich and supports high rates of primary productivity (Lowry et al., 2015). As such, this region supports high concentrations of benthic macrofaunal biomass of up to 25 g C m^{-2} (Grebmeier et al., 2015). Station 12 had similar bottom water DIC and salinity characteristics as stations 2 and 14 in the Bering Sea, while stations 4 and 9 (eastern Chukchi Sea) had higher bottom water DIC and salinity by about 100–200 μmol kg^{-1} and 1, respectively, than the other three stations (Table 1). Stations 4 and 9 are in the eastern Chukchi Sea, north of Cape Lisburne, AK. Stations 4, 9, and 12 are all influenced by the nutrient-rich BSAW at the surface, indicated by SSS >30.5 (Pisareva et al., 2015). Both stations 4 and 9 had initial NO_3^- and Si bottom water concentrations which were significantly higher than the three more southerly stations. The initial conditions in the eastern Chukchi Sea bottom waters are representative of newly-ventilated and remnant winter waters which are cold and saline and have accumulated remineralization products from benthic respiration and the northward flow of Pacific-sourced winter waters (Pisareva et al., 2015). Accordingly, bottom water pH_T was lower by ~0.2 units at these northern Chukchi Sea stations as well.

The spatial and temporal resolution of this study captured a broad range of ice coverage characteristics (Fig. S3). Stations 2 and 14 in the Bering Sea had been fully ice-free for over a month at the time of sampling. Station 12 just north of the Bering Strait had been ice-free for about one month, though the surrounding waters still had minimal ice coverage of less than 25% (NSIDC Sea Ice Index, Fetterer et al., 2017). Stations 4 and 9 in the northeastern Chukchi Sea were in an area of active sea ice retreat. Station 4 was partially ice-covered with a sea-ice concentration of at least 50% in the weeks preceding sampling. In contrast, station 9 was at least 75% ice-covered for several weeks prior to sampling and represents the best baseline in our study for sediment-water fluxes at the end of the ice-covered season.

3.2. Solute concentration changes during incubations

Fig. 2 shows the trends in DIC, pH_T, silicate (Si), TA, and Ω_{arag} in the overlying water throughout the incubation for each replicate sediment core. At some sites, replicate cores had similar rates of solute change, but others (particularly stations 12 and 14) had distinctly different trends in DIC change, likely due to greater macrofaunal irrigation in one of the replicates. A similar pattern is apparent in ^{222}Rn and silicate fluxes, as both solutes had higher fluxes in the replicate with higher DIC flux. The ^{222}Rn profiles are not shown, as ^{222}Rn fluxes are based on a single sampling about 2 days after each incubation began.

For all stations, DIC increased consistently over time. While DIC rates of change were highly variable among core replicates, similar trends were consistent across independent biogeochemical measurements. For example, variations in DIC concentrations among replicate cores agreed well with corresponding differences independently observed in pH_T measurements (Fig. 2a and b). These differences can be strongly modulated by infaunal activity, and the replicate heterogeneity illustrates the range of sedimentary processes observed at small spatial scales in this region (e.g., Souza et al., 2014). Table 2 summarizes the sediment characteristics and qualitative visual identification of infauna for each core. We acknowledge that our core replicates may not fully capture the entire range of solute fluxes that can occur at a given station. Therefore, we recommend using multiple replicates for future benthic flux determinations in this region to ensure a more comprehensive understanding of solute flux variability.

The tight coupling between DIC increase and pH_T decrease over time at all stations indicates that organic matter respiration, producing CO_2 and H^+, was the dominant control on carbonate system changes. The production of H^+ in pore waters resulting from benthic respiration is often coupled with sedimentary carbonate dissolution (Brenner et al., 2016). Because DIC efflux results from dissolved CO_2, bicarbonate, and carbonate, the DIC efflux resulting from respiration is not due to the signal of organic matter remineralization alone, but rather to the combined processes of respiration and carbonate dissolution.

Due to the decreasing pH_T with time resulting from respiration, the carbonate pool shifted to bicarbonate, resulting in a stark decrease in Ω_{arag} over time (Fig. 2e). Notably, the initial Ω_{arag} at all stations was

Table 1
Initial biogeochemical conditions of the overlying water in each sediment core incubation. From left to right, stations are ordered north to south. Initial samples were drawn when temperatures were stabilized, ~2–3 h after collection, which may partially explain the slight variability of replicates.

Sample	2A	2B	14A	14B	12A	12B	4A	4B	9A	9B
Latitude [dd]	62.00		63.00		67.00		69.00		69.76	
Longitude [dd]	-168.54		-167.37		-168.00		-167.35		-166.93	
Water column depth [m]	33		39		34		47		46	
Salinity	31.50		31.22		31.24		32.52		33.25	
Temp. [°C]	1.60		0.04		0.82		1.69		1.75	
DIC (SD) [μmol kg^{-1}]	1999.6 (2.5)	2008.8 (2.2)	2015.7 (2.0)	2011.5 (1.4)	1979.5 (1.5)	1972.8 (1.1)	2135.9 (2.7)	2151.2 (1.0)	2248.8 (9.5)	2242.7 (4.8)
TA (SD) [μmol kg^{-1}]	2069.2 (4.0)	2082.5 (3.9)	2135.8 (4.5)	2124.6 (4.4)	2212.1 (4.5)	2115.7 (8.3)	2199.7 (4.2)	2210.3 (3.1)	2309.0 (3.5)	2304.7 (4.0)
pH_T	7.874	7.887	8.041	8.032	8.112	8.119	7.839	7.837	7.819	7.826
NO_3^- (SD) [μmol L^{-1}]	5.14 (0.05)	4.44 (0.02)	1.32 (0.12)	0.95 (0.14)	1.48 (0.12)	1.35 (0.04)	11.46 (0.04)	10.78 (0.11)	15.98 (0.10)	15.05 (0.07)
NH_4^+ (SD) [μmol L^{-1}]	2.81 (0.18)	2.11 (0.00)	0.22 (0.02)	0.64 (0.09)	0.00 (0.00)	0.00 (0.00)	1.36 (0.17)	1.48 (0.04)	2.04 (0.02)	1.77 (0.26)
PO_4^{3-} (SD) [μmol L^{-1}]	1.08 (0.03)	1.05 (0.02)	0.67 (0.01)	0.71 (0.00)	0.75 (0.01)	0.78 (0.01)	1.60 (0.01)	1.50 (0.00)	1.65 (0.02)	1.50 (0.00)
Si (SD) [μmol L^{-1}]	12.4 (0.3)	13.3 (0.3)	1.4 (0.0)	1.4 (0.0)	1.8 (0.0)	1.6 (0.0)	27.7 (0.6)	27.6 (0.6)	34.4 (0.7)	34.4 (0.7)
Ω_{arag} (SD)	0.96 (0.07)	1.00 (0.07)	1.39 (0.10)	1.32 (0.09)	1.57 (0.11)	1.57 (0.11)	0.96 (0.07)	0.92 (0.07)	0.96 (0.07)	0.97 (0.07)

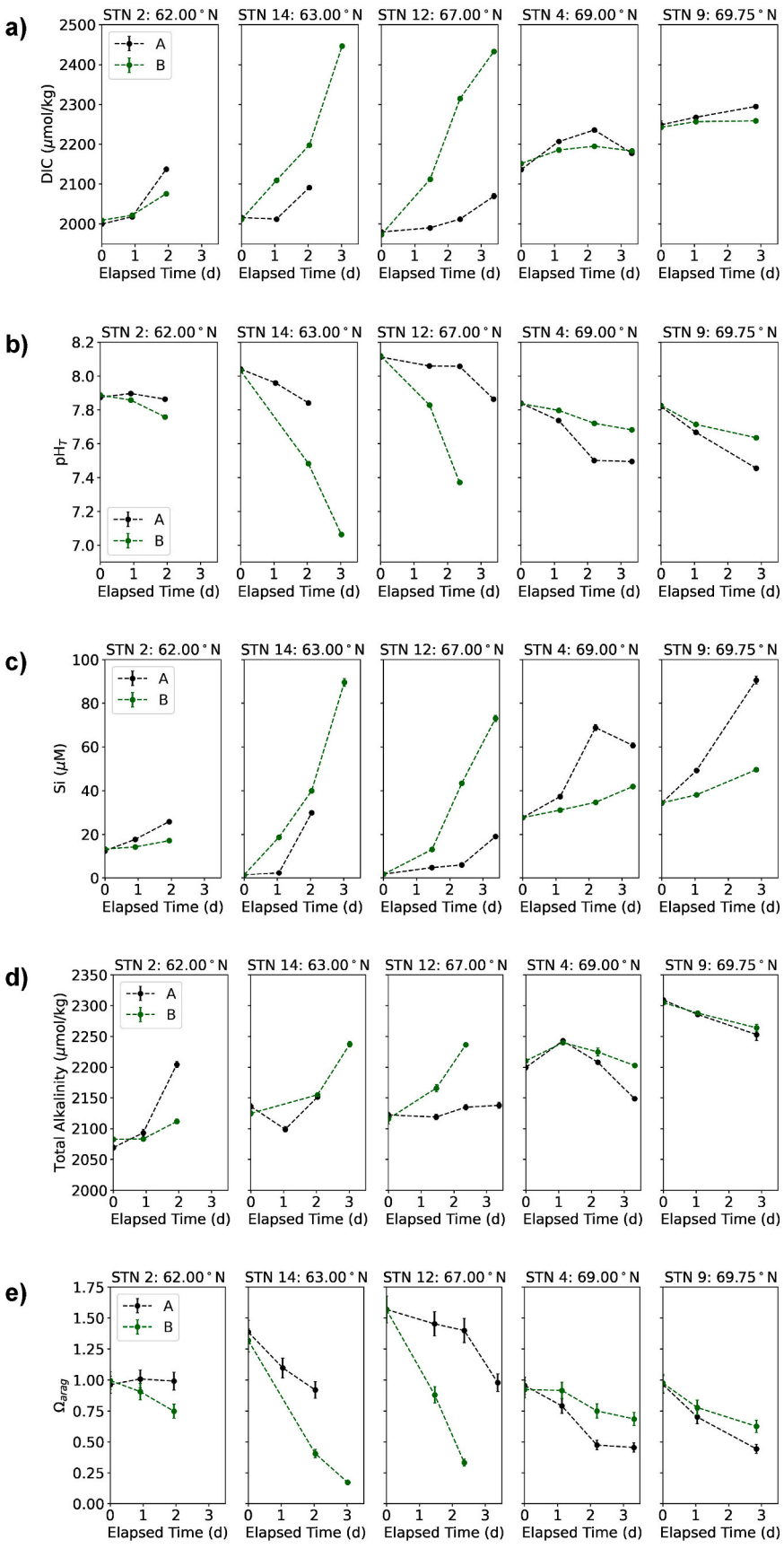

Fig. 2. (a) DIC, (b) pH_T, (c) silicate, (d) TA, and (e) Ω_{arag} changes over time in overlying water for each station. In each subplot, replicate A is shown in black and replicate B in green. Note that DIC, pH_T, and Si are direct measurements, while TA and Ω_{arag} were calculated using CO2SYS. Y-axis error bars show the analytical uncertainty of triplicate analyses for measured parameters (a–c), or the propagated uncertainty for calculated parameters (d–e). Slopes of these plots reflect both benthic flux and the height of water above the sediment, which decreased due to sampling as the incubation progressed. Fluxes were calculated from the regressions shown in Supplemental Fig. 2.

Table 2
Sediment core descriptions. From top to bottom, stations are ordered south to north. Sediment descriptions and infauna identification are visual and qualitative and were conducted at the end of the incubation.

Core	Latitude (dd)	Longitude (dd)	Core length (cm)	Sediment description	Infauna observations
2 A	62.00	−168.54	14	Muddy, 3 open burrows at the top	Live cnidarian (~1 cm diameter, see Fig. S2) emerged ~7 cm from a burrow during the incubation.
2 B			12	Muddy	–
14 A	63.00	−167.37	33	Light brown silty sand at top few cm, transition to gray, then black at depth, several empty burrows	Putative polychaete tubes (rigid, conical tubes, ~2 cm long, <1–2 mm diameter, orange-tinted), found at the surface. Thin red worms, clam shells at various depths, and a large gastropod at 25 cm.
14 B			33	Similar characteristics as 14 A	>15 conical tubes as in 14 A at the surface. Red worms and burrows to 20 cm depth.
12 A	67.00	−168.00	25	Fine brown mud, 3 burrows at the top	8-10 live arthropods (~5 mm long), a few immobile thin red worms (possibly dead) at the surface. Live mollusc at 6 cm.
12 B			25	Fine brown mud, 2 burrows at the top. Darker mud below 2 cm. Open burrow with oxidized margin at 22 cm.	3 thin red worms near surface, cnidarian in a burrow near surface, small mollusc at 1 cm, larger mollusc at 2 cm. Two small arthropods at 9 and 16 cm.
4 A	69.00	−167.35	26	Muddy, upper 1 cm flocculent and core bottom stiff. Many pockmarks at the surface, possible amphipod burrows	Small echinoderm and two small molluscs at the surface. <1 mm diameter red worms at 25 cm.
4 B			24	Similar characteristics as 4 A	Small echinoderm and a few red worms at the surface.
9 A	69.76	−166.93	25	Brown mud with 6 burrows at the surface. Regions of black, reduced sediment at depth. Many burrows at depth.	One live worm and >10 small arthropods (<3 mm) at the surface.
9 B			25	Similar characteristics as 9 A, few pebbles at the surface. Red coloration (iron oxides) at 20 cm surrounding an indurated tube.	Mollusc shells at 20 cm. Putative bryozoan at surface. Small thin worms at depth.

<1.5, and aragonite always became undersaturated ($\Omega_{arag} < 1$) through the course of the incubation. The low bottom water Ω_{arag} observed here is consistent with previous observations of bottom water $\Omega_{arag} < 2$ in the Bering and Chukchi Seas due to waters influenced by the shoaling of deep Pacific waters, benthic respiration, and low-alkalinity riverine input, leading to high DIC/TA (Mathis et al., 2011; Yamamoto-Kawai et al., 2016; Sun et al., 2021).

NO_3^- and NH_4^+ had less consistent trends across cores (Fig. S2), which may reflect differences in the dominant nitrogen utilization and production pathways in the surface sediments and in the water column. The rate of change in NH_4^+ often increased after 3–4 days of incubation, likely indicating a more reducing, low-oxygen condition in the cell. As porewater nitrogen speciation was not measured, it is unclear whether transformations between organic N, NO_3^-, and NH_4^+ occurred in the sediments or in the overlying water. For that reason, nitrogen fluxes are considered here as the total dissolved inorganic nitrogen (DIN), the combination of NO_3^- and NH_4^+ fluxes (nitrite concentrations were non-detectable).

3.3. Sediment-water fluxes

Solute fluxes from the sediment to the overlying water were calculated as a linear regression of the first three time points of water concentration versus the time to height ratio (Fig. S2). Excluding incubation time points beyond ~3.5 days (~25 days m^{-1}) minimized closed-system artifacts of long-term incubation. Fig. 3 shows the fluxes from sediments to the water column for selected biogeochemical parameters. Positive values indicate a flux from the sediment to the overlying water (efflux), while negative values indicate a flux from the water into the sediment (influx).

3.3.1. Carbonate system fluxes – DIC and TA

The three southernmost stations had the greatest and most variable DIC fluxes (Fig. 3a), between 1 and 25 mmol m^{-2} d^{-1}, as compared to the two northernmost stations which always had fluxes <10 mmol m^{-2} d^{-1} and mostly <5 mmol m^{-2} d^{-1}. DIC, pH_T, phosphate, silicate, and salinity measurements were used to compute total alkalinity (TA) fluxes (Fig. 3b). TA fluxes also displayed spatial heterogeneity, with stations 2 and 12 (Bering Shelf and southern Chukchi Sea) having high and variable fluxes of 0–13 mmol m^{-2} d^{-1} in contrast to stations 14 and 4 (northern Bering and eastern Chukchi Seas) which had lower fluxes of 1.5–3.0 mmol m^{-2} d^{-1}. TA efflux corresponded positively to DIC efflux ($r = 0.74$, $p = 0.015$, $n = 10$). The source of the DIC from these sediments is likely respiration of organic carbon, with additional contributions from dissolution of shell carbonate, which also contributes to TA efflux. The maximum source of shell carbonate can be estimated based on the alkalinity flux, divided by 2 μeq/μmol. However, some of the alkalinity flux might also reflect oxidation of organic carbon through sulfate or ferric oxide reduction, coupled with precipitation of iron sulfides. Assuming the alkalinity flux reflects carbonate dissolution alone, the DIC flux from organic carbon oxidation should be greater than 4–11

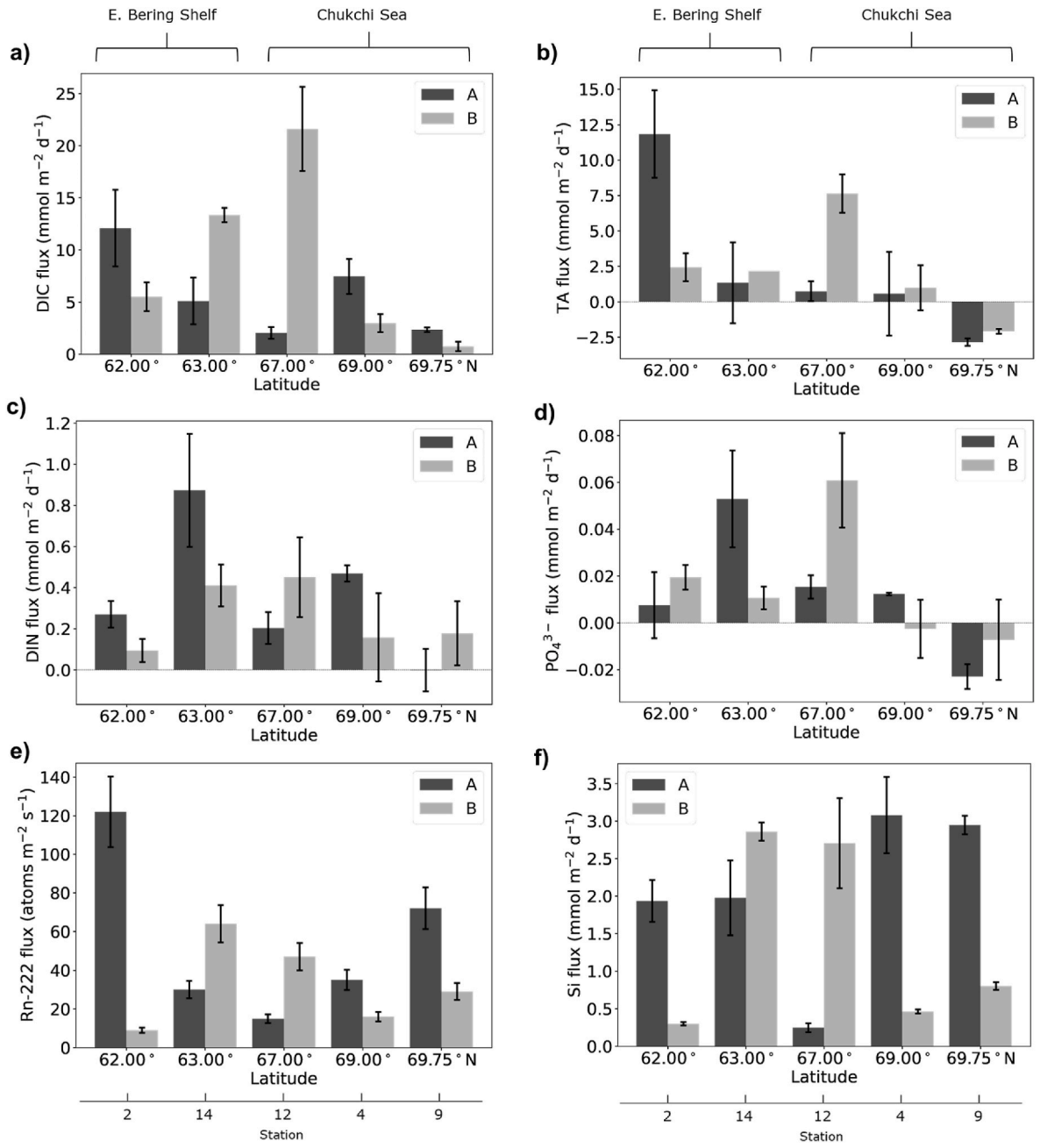

Fig. 3. Parameter fluxes calculated over the first 3 days of incubation for a) DIC, b) TA, c) DIN, d) PO_4^{3-}, e) Rn-222, and f) Si. Dark and light gray bars represent two core replicates at a given station. Y-axis error bars represent the standard error of the linear regression used to calculate flux. Note the different y-axis scales for each subplot.

mmol m^{-2} d^{-1} and 2–18 mmol m^{-2} d^{-1} at stations 12 and 14, respectively.

Sediment-water effluxes of organic matter remineralization products such as DIC, DIN, and Si were lower in the eastern Chukchi Sea, likely due to a combination of lower export production and inhibited air-sea exchange, causing the accumulation of DIC, DIN, and Si in the water column. Though these are the first directly measured benthic DIC fluxes reported for this region, they are similar to or slightly lower than those reported in the Baltic Sea region (~15–60 mmol m^{-2} d^{-1}, Hall et al., 2017), lower than those reported in subtropical environments (~15–100 mmol m^{-2} d^{-1}, Alongi et al., 2011), and slightly higher than those reported in the Barents Sea (<2 mmol m^{-2} d^{-1}, Freitas et al., 2022). Assuming that our DIC fluxes primarily result from organic matter respiration and concurrent carbonate dissolution, these comparisons are consistent with the expectation that benthic respiration is higher in low-latitude environments and decreases poleward, as temperature strongly modulates benthic respiration rates (Hancke and Glud, 2004). However, despite the relatively consistent bottom water temperature across the study region, DIC fluxes showed a strong spatial variation across the study area. While temperature plays an important role in benthic respiration, the supply of organic matter to the sediments (O'Daly et al., 2020) and the benthic macrofaunal composition (Grebmeier et al., 2015) are heterogeneous in this region and important additional controls on the observed spatial variation in fluxes.

Our reported DIC fluxes for the eastern Chukchi Sea agree reasonably well with springtime benthic carbon respiration rates derived from sediment oxygen demand (SOD) in the western Arctic Ocean (~0.5–5 mmol C m^{-2} d^{-1}, Moran et al., 2005). In the decade 2000–2010,

Grebmeier (2012) observed elevated sediment oxygen consumption relative to the northern Chukchi Sea in the Hope Sea Valley (near our station 12) of ~25 mmol m^{-2} d^{-1}. Assuming a ratio of 138 mol of O_2 consumed for every 106 mol of CO_2 produced in microbial respiration (Redfield, 1934), this corresponds to a DIC efflux of ~19 mmol m^{-2} d^{-1}, which agrees with our DIC flux observations of 2–21.6 mmol m^{-2} d^{-1} at this station. The agreement between our direct DIC flux measurements and those calculated from SOD indicates that SOD can still be reasonably used to estimate the benthic inorganic carbon contribution. This would be advantageous as SOD measurements are more readily available for this region (Grebmeier, 2012). However, the observed heterogeneity of DIC fluxes in comparison to oxygen merits further study to constrain the uncertainty of both direct carbon flux measurements and of their estimation from SOD. Additionally, it should be noted that the mechanisms of inorganic carbon and oxygen effluxes from sediments differ such that SOD cannot fully constrain benthic respiration, especially in oxygen-deficient sediments where processes other than aerobic respiration produce significant amounts of CO_2 at depth which can be mobilized by infauna (Aller, 2004).

The eastern Chukchi Sea had been covered by ice as recently as one day prior to sampling (Fig. S1) while the southern Chukchi and northern Bering Seas had been ice-free for several weeks longer. During the ice-covered season, two important sinks for water column CO_2 are inhibited: 1) ice coverage causes light limitation of primary productivity while heterotrophs remain active (Garneau et al., 2007), and this is reflected in the high initial DIC concentrations at stations 4 and 9, and 2) sea ice coverage slows (but does not fully inhibit) air-sea gas exchange (Semiletov, 1999). During winter, DIC accumulates in the water column in areas of ice coverage, though pCO_2 remains undersaturated due to the elevated solubility of CO_2 in cold water (Bates, 2006). The bottom waters of the eastern Chukchi Sea are also influenced by the flow of cold, saline Bering Sea winter water which is rich in remineralization products (Pisareva et al., 2015). The eastern Chukchi Sea also has relatively low export production, benthic biomass, and sediment oxygen demand (O'Daly et al., 2020; Grebmeier et al., 2015; Grebmeier, 2012). Elevated water column DIC was observed in the eastern Chukchi Sea at the time of sampling, likely due to the retreat of sea ice only a few hours or days prior. The eastern Chukchi Sea is a CO_2 sink on an annual basis and sea ice retreat leads to intense phytoplankton blooms which serve to draw down CO_2 (Bates, 2006). Our observations, particularly at ice-covered station 9, captured the sediment-water relationship prior to significant surface water DIC drawdown and organic matter production, wherein sediment-water DIC fluxes were low due to low springtime respiration rates.

DIC fluxes showed a negative correlation with the overlying water DIC concentration; higher effluxes were observed in areas with lower bottom water DIC (Fig. 4, $r = -0.98$, $p = 0.003$, $n = 5$ when flux replicates are averaged). The eastern Chukchi Sea had the highest bottom water DIC concentrations of ~2140 and 2245 μmol kg^{-1} for stations 4 and 9, respectively, as compared to ~1975–2015 μmol kg^{-1} in the southern stations. While the strong relationship between overlying water (OLW) DIC and DIC efflux may indicate diffusive flux limitations, it is also possible that this correlation reflects the reduced rate of organic carbon export in the northerly stations. This would indirectly lead to the correlation between DIC and DIC flux due to a lack of DIC drawdown in the water column and lack of labile material supplied to the benthos to fuel respiration.

3.3.2. *Nutrient effluxes and relationships with DIC*

In contrast to the eastern Chukchi Sea, relatively high effluxes of remineralization products from the sediments were observed in the southern Chukchi Sea at station 12, which had been ice free for over 30 days. This station is in an area of high macrofaunal benthic biomass with concentrations up to 25 g C m^{-2} (Grebmeier et al., 2015) owing to the influx of nutrient-rich Pacific waters and subsequent high rate of export productivity following sea ice retreat (Lowry et al., 2015). In this region,

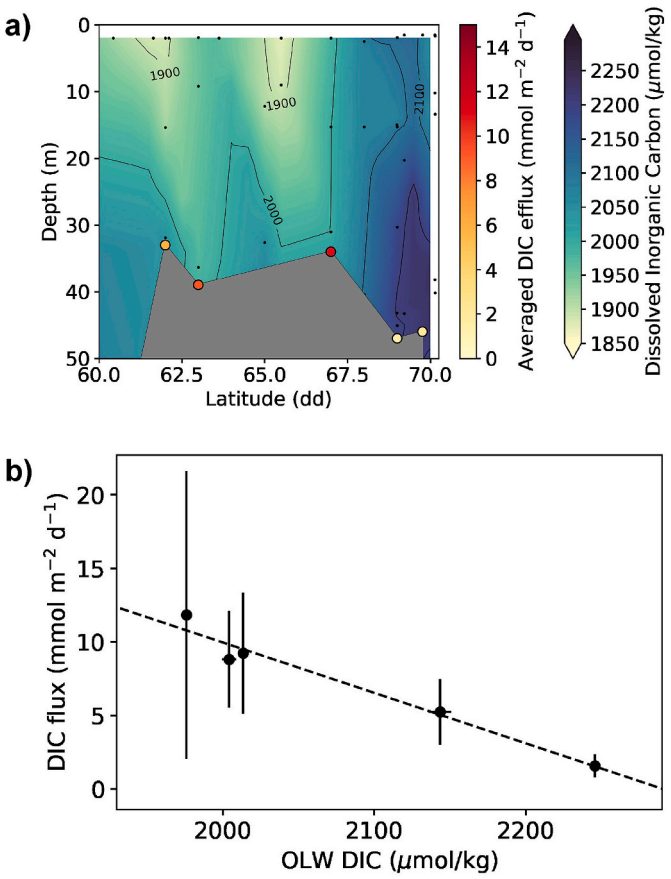

Fig. 4. (a) An interpolated longitudinal cross-section of water column DIC values observed in the study region (background blue-green color bar), overlain by the corresponding efflux of DIC from the sediments (orange-red colored dots). (b) The relationship between DIC efflux and the overlying water concentration (OLW DIC) with a linear trendline. Here flux replicates are averaged and the error bars show the standard deviation for replicates. For the linear regression, Pearson's $r = -0.98$, $p = 0.003$, $n = 5$.

macrofaunal biomass has also been associated with greater sediment-water ammonium efflux indicating active benthic respiration (Henriksen et al., 1990). Accordingly, the high fluxes of the remineralization products DIC, DIN, and PO_4^{3-} observed at station 12 were similar to those observed in the Bering Sea (Fig. 3).

Although the oxidation of organic matter estimated from DIC flux (using alkalinity flux to estimate possible carbonate dissolution) provides only a lower limit, it is still worthwhile to estimate the ratio of this parameter to total N flux (Fig. 5a). While the ratio for one core (14 A) is comparable to the Redfield ratio of 6.6, most other cores have significantly higher ratios. This suggests that a large fraction of the N fixed by phytoplankton is lost to denitrification. The highest ratios of DIC to DIN fluxes were observed on the Bering Shelf, especially at station 2. This is consistent with previous observations of coupled nitrification and denitrification on the Bering Shelf and enriched $\delta^{15}N$ of surface sediment in the early spring (Granger et al., 2011), as well as high rates of sediment denitrification (accounting for 4–13% of the global total) in Chukchi Sea sediments under areas of high export production, regardless of ice coverage (Chang and Devol, 2009; Hardison et al., 2017).

The eastern Chukchi Sea (station 9) was the only station with a net PO_4^{3-} influx, though it was small, −0.03 mmol m^{-2} d^{-1} (Fig. 3d). This was also the only station that had a net TA influx to the sediment of ~ −2 mmol m^{-2} d^{-1} despite a modestly positive DIC flux. Marine sedimentary phosphate uptake is often associated with the presence of ferric oxides (Sundby et al., 1992). If the negative alkalinity fluxes at this site reflect oxidation of iron sulfides, ferric oxides are likely forming and

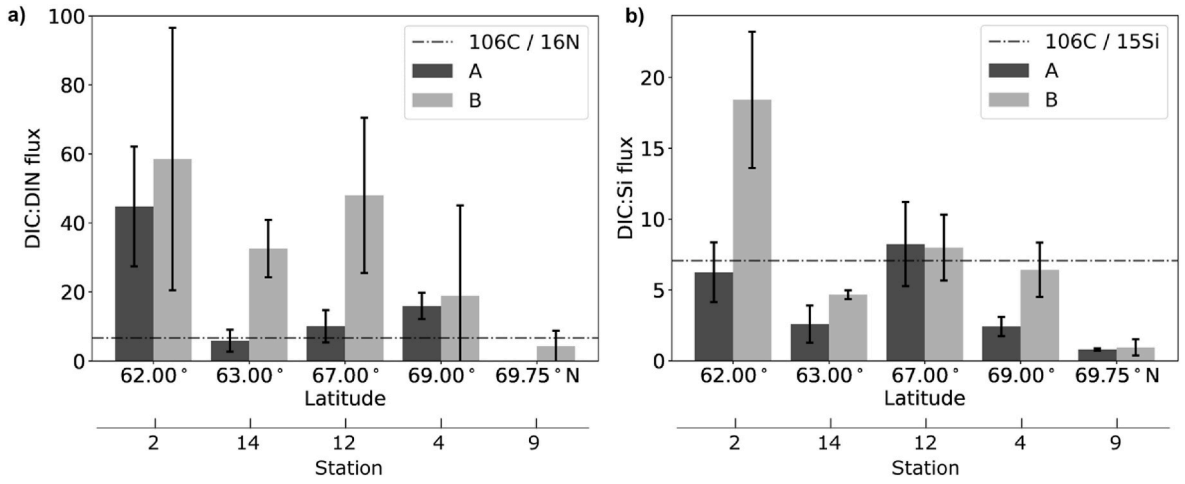

Fig. 5. (a) The ratio of DIC to DIN ($=NO_3^- + NH_4^+$) fluxes and (b) the ratio of DIC to Si fluxes (both measured in mmol m^{-2} d^{-1}) for each core replicate with latitude. The dash-dotted line shows the expected elemental ratio for organic matter remineralization (106C:16 N:15Si, Redfield, 1934; Brzezinski, 1985). Error bars show the propagated error of the standard errors of the linear regressions used to calculate each individual flux. Note the different y-axis scales in each subplot.

adsorbing phosphate. However, the mechanisms are difficult to evaluate without solute pore water profiles.

The fluxes of the remineralization products DIC, DIN, and PO_4^{3-} all decreased northward in the Chukchi Sea (Fig. 3). This was concurrent with a northward trend of increasing bottom water concentrations of these parameters. The decreasing northward fluxes most likely reflect the lower rates of benthic respiration and the relationship between ice retreat and benthic-pelagic coupling. Ice retreat allows for light penetration and nutrients accumulated over the winter to fuel primary productivity, increasing the export of labile organic matter to the sediments and fueling benthic respiration. One measure of this is the DIC/Si flux ratio (Fig. 5b). A higher DIC/Si ratio indicates respiration of more labile material, as benthic microbes will preferentially consume the more carbon-rich material. As the supply of diatoms to sediments decreases, the DIC/Si flux ratio should decrease as the more refractory material containing more Si is consumed. The DIC/Si flux ratio showed considerable geographic variation, with high values in the southernmost stations which had been ice-free for at least one month, and low values in recently ice-free northern sites (station 9). This reflects the more rapid decomposition of organic C relative to biogenic Si (Conley et al., 1993), as recently ice-free sediments are still dissolving some of previous year's deposited diatom Si but have exhausted the labile carbon supply. In the northeastern Chukchi Sea, export fluxes primarily composed of diatoms are low during the winter season and begin to peak during June as sea ice retreats (Lalande et al., 2020). As sea ice retreats, the flux of sympagic algae to sediments increases (Lalande et al., 2020), and low rates of zooplankton grazing maintain high export ratios (Campbell et al., 2009). The northward decrease in the DIC/Si flux ratio is consistent with the expectation that greater ice coverage inhibits the export of fresh diatoms to the benthos.

3.3.3. *Radon-222 and the role of bio-irrigation*

Radon-222 (^{222}Rn) is a radioactive noble gas produced by the α-decay of radium-226 (^{226}Ra).^{226}Ra is highly particle-reactive and sorbs to sediments. By contrast, its decay product ^{222}Rn is water-soluble and can readily dissolve into porewaters. As a noble gas, ^{222}Rn is biologically inert, so its only source is decay of ^{226}Ra and its only sinks are radioactive decay and physical transport from its source region. ^{222}Rn is transferred from porewater to the overlying water by both diffusive and non-diffusive transport. When organisms actively irrigate sediments, the diffusive flux is augmented, offering an indication of the extent of irrigation activities (Callender and Hammond, 1982). The ^{222}Rn data allow us to resolve the contribution of bio-irrigation as compared to molecular diffusion as mechanisms of solute efflux (see Supplemental Information).

Rn emanation rates from solid phases were measured (2 horizons from one core per station) and used to predict diffusive fluxes. Results indicated that the lower Rn fluxes observed (Fig. 3e) were comparable to predicted diffusive fluxes (~18–27 atoms m^{-2} s^{-1}), while larger fluxes indicated substantial bio-irrigation. The most extreme example occurred during incubation of core 2 A, as a small cnidarian gradually emerged from the sediments (Fig. S1). The Rn flux for this core was more than 6 times the predicted diffusive flux, indicating the substantial influence of bio-irrigation on sediment-water solute flux for this sample. Following incubations, cores were cut open and examined, and a variety of bio-irrigating infauna were visually identified in nearly all cores (Table 2). The dominant role of macrofauna in benthic-pelagic coupling in this region has been well-demonstrated (Grebmeier et al., 1989), and our study directly quantifies this effect with regard to the sedimentary efflux of inorganic carbon.

In general, when replicate cores at each station are compared, the fluxes of ^{222}Rn (Fig. 3e) correspond well to those of the remineralization products DIC (Fig. 3a), DIN (Fig. 3c), and Si (Fig. 3f). However, the ratios of ^{222}Rn and DIC effluxes were quite different across stations. For example, at station 9, DIC efflux was low (<5 mmol m^{-2} d^{-1}) despite a relatively high ^{222}Rn efflux of 29–72 atoms m^{-2} s^{-1} that indicated bio-irrigation by infauna. Variations in Rn emanation rate from solid phases are modest in the study area (Supplemental Information), and there does not seem to be a strong geographic difference in average benthic Rn fluxes (Fig. 3e). Consequently, despite infaunal activity promoting solute mobility, the low average DIC efflux in the northern regions implies that there were low concentrations of DIC in the porewater and/or that the relatively high concentration of DIC in the overlying water inhibited significant efflux, as supported by the results in Fig. 4b. In contrast, at station 12 DIC efflux was high (2.0–21.6 mmol m^{-2} d^{-1}) despite relatively lower ^{222}Rn efflux (15–47 atoms m^{-2} s^{-1}). This indicates that the regional contrast in DIC flux is not simply due to a pattern of bio-irrigation, but should reflect a contrast in the production of DIC in sediment.

3.4. *Implications*

As the Arctic atmosphere continually warms from the effect of anthropogenic greenhouse gases, the spring ice-melt season is projected to begin earlier, and ice growth to begin later (Stroeve et al., 2014), with fully ice-free Septembers predicted for as early as the 2030's (Wang and Overland, 2009). Our study demonstrates the indirect role of ice coverage and export production on the sedimentary efflux of

remineralization products in the Bering and Chukchi Seas. Spring phytoplankton blooms are important for export production and carbon sequestration in this region, but benthic respiration can modulate how much exported carbon is stored in sediments, exported to adjacent basins, or re-released to the water column. The long-term effects of an earlier melt-season and increased Pacific water inflow (Woodgate, 2018) on Arctic productivity are not clear, but the data presented here indicate that the greatest efflux of remineralization products is associated with regions of high export production influenced at the surface by nutrient-rich Pacific water (O'Daly et al., 2020). While many studies justifiably focus on surface water productivity and air-sea exchange to estimate carbon uptake in the Bering and Chukchi Seas, we emphasize that the benthos is an important component for carbon uptake, storage, and re-release in these shallow shelves that exhibit extensive benthic-pelagic coupling. The dramatic export production coupled with low grazing pressure in these Arctic marginal seas causes a majority of organic matter consumption and CO_2 production to occur in the sediments. The paucity of sediment-water inorganic carbon flux data has been addressed with estimates based on oxygen flux, but the differences in their formation processes complicate a direct comparison. Our results show that while previous calculations of DIC efflux based on sediment oxygen consumption are reasonably similar to observations, the small-scale spatial heterogeneity of infauna plays a significant role in carbon cycling, especially in areas with high export production. The dominant role of sediments in organic carbon remineralization in this region merits further investigation of spatial, seasonal, and temporal trends in sedimentary carbon dynamics, which could have important implications for refining our understanding of the role of shallow marginal seas of the Arctic in global climate.

4. Summary

This work captured sediment-water fluxes of inorganic carbon and nutrients across a range of sea ice coverage and surface productivity regimes. To our knowledge, we present the first direct measurements of inorganic carbon sediment-water fluxes in the Bering and Chukchi Seas. Across the study area, the sediments were a source of the remineralization products DIC, DIN, and Si to the water column. However, the ratios of oxidized organic C to total N flux are typically far above the expected Redfield ratio of 6.6, indicating that substantial denitrification must occur in sediments. In the Chukchi Sea, bottom water nutrient concentrations generally increased and sedimentary effluxes generally decreased northward. This pattern likely reflects the onset of water column export of carbon and nutrients as spring conditions move northward. Moving northward in the Chukchi Sea, the water column had greater ice coverage, inhibiting surface productivity and air-sea exchange. Thus, we expect our northernmost stations, in the eastern Chukchi Sea, near Cape Lisburne, AK, to be most representative of baseline low wintertime sediment-water flux conditions under low export production, while the more southerly stations represent springtime benthic fluxes when productivity has been high and there is more extensive benthic-pelagic coupling. While these values may serve as a seasonal reference, they may also demonstrate how sedimentary fluxes may evolve under future conditions wherein sea ice retreats earlier in the season. We note that replicate sample cores often displayed highly heterogeneous results, which in part illustrates the dynamic nature of the benthic environment in this region, especially in the most productive areas with the highest concentration of bio-irrigating benthic macrofauna. To further constrain the effects of early-season ice retreat on sediment-water fluxes of inorganic carbon, future work is recommended under a range of ice-coverage and export productivity conditions, including time-series sediment flux analyses at a single location.

Declaration of competing interest

The authors declare that they have no known competing financial interests or personal relationships that could have appeared to influence the work reported in this paper.

Data availability

Data will be made available on request.

Acknowledgments

This work was supported by NSF Grant #2049991 (P. Vlahos) and NSF Grant #1854454 (R. Mason). We thank the University of Alaska for the coordination of the cruise and shipboard access. We thank the Captain and crew of the *R/V Sikuliaq* for shipboard support. We also thank Dr. Claudia Koerting and the University of Connecticut SMALER lab for assistance in laboratory analyses. At USC, Ben Melechin and Luke Holmes assisted with measurements of sediment properties. Finally, we thank the anonymous reviewers for their thorough review and helpful suggestions to improve this manuscript.

Appendix A. Supplementary data

Supplementary data to this article can be found online at https://doi.org/10.1016/j.csr.2023.105116.

References

Aller, R.C., 2004. Conceptual models of early diagenetic processes: the muddy seafloor as an unsteady, batch reactor. J. Mar. Res. 62, 815–835. https://doi.org/10.1357/0022240042880837.

Alongi, D.M., Trott, L.A., Mohl, M., 2011. Strong tidal currents and labile organic matter stimulate benthic decomposition and carbonate fluxes on the southern Great Barrier Reef shelf. Continent. Shelf Res. 31, 1384–1395. https://doi.org/10.1016/j.csr.2011.05.018.

APHA, 1997. Standard Method 4500-NH3 Nitrogen (Ammonia), pp. 108–117.

APHA, 1999. Standard Method 4500-P Phosphorus (Phosphate), pp. 146–162.

APHA, 2011. Standard Method 4500-NO3 Nitrogen (Nitrate), pp. 120–129.

APHA, 2013. Standard Method 4500-NO2 Nitrogen (Nitrite), pp. 85–87.

Armante, C., Eakins, B.W., 2009. ETOPO1 Arc-Minute Global Relief Model: Procedures, Data Sources and Analysis, vol. 24. NOAA Technical Memorandum NESDIS NGDC, p. 19.

Arrigo, K.R., van Dijken, G.L., 2011. Secular trends in Arctic Ocean net primary production. J. Geophys. Res. 116, C09011 https://doi.org/10.1029/2011JC007151.

Arrigo, K.R., et al., 2012. Massive phytoplankton blooms under arctic Sea Ice. Science 336, 1408. https://doi.org/10.1126/science.1215065.

Bates, N.R., 2006. Air-sea CO_2 fluxes and the continental shelf pump of carbon in the Chukchi Sea adjacent to the Arctic Ocean. J. Geophys. Res. 111, C10013 https://doi.org/10.1029/2005JC003083.

Berelson, W.M., Hammond, D.E., Eaton, A., 1987. A technique for the rapid extraction of radon-222 from water samples and a case study. In: Graves, B. (Ed.), Radon, Radium and Other Radioactivity in Groundwater. Lewis Pub., Chelsea, MI, pp. 271–281.

Brenner, H., Braeckman, U., Le Guitton, M., Meysman, F.J.R., 2016. The impact of sedimentary alkalinity release on the water column CO_2 system in the North Sea. Biogeosciences 13, 841–863. https://doi.org/10.5194/bg-13-841-2016.

Brzezinski, M.A., 1985. The Si:C:N ratio of marine diatoms: interspecific variability and the effect of some environmental variables. J. Phycol. 21 (3), 347–357. https://doi.org/10.1111/j.0022-3646.1985.00347.x.

Cai, W.-J., et al., 2010. Decrease in the CO_2 uptake capacity in an ice-free Arctic Ocean basin. Science 329, 556–559. https://doi.org/10.1126/science.1189338.

Callender, E., Hammond, D.E., 1982. Nutrient exchange across the sediment-water interface in the potomac river estuary. Estuar. Coast Shelf Sci. 15, 395–413. https://doi.org/10.1016/0272-7714(82)90050-6.

Campbell, R.G., Sherr, E.B., Ashijan, C.J., Plourde, S., Sherr, B.F., Hill, V., Stockwell, D. A., 2009. Mesozooplankton prey preference and grazing impact in the Western Arctic Ocean. Deep-Sea Res. II 56, 1274–1289. https://doi.org/10.1016/j.dsr2.2008.10.027.

Chang, B.X., Devol, A.H., 2009. Seasonal and spatial patterns of sedimentary denitrification rates in the Chukchi sea. Deep-Sea Res. II 56, 1339–1350. https://doi.org/10.1016/j.dsr2.2009.10.024.

Clayton, T.D., Byrne, R.H., 1993. Spectrophotometric seawater pH measurements: total hydrogen ion concentration scale calibration of m-cresol purple and at-sea results. Deep-Sea Res. 40, 2115–2129. https://doi.org/10.1016/0967-0637(93)90048-8.

Coachman, L.K., Aagaard, K., Tripp, R.B., 1981. A diffusion model of cross-shelf exchange of nutrients in the southeastern Bering Sea. Deep-Sea Res. 28A (8), 819–846. https://doi.org/10.1016/S0198-0149(81)80003-9.

Conley, D.J., Schelske, C.L., Stoermer, E.F., 1993. Modification of the biogeochemical cycle of silica with eutrophication. Mar. Ecol. Prog. Ser. 101, 179–192. https://doi.org/10.3354/meps101179.

DeGrandpre, M., Evans, W., Timmermans, M.-L., Krishfield, R., Williams, B., Steele, M., 2020. Changes in the Arctic Ocean carbon cycle with diminishing ice cover. Geophys. Res. Lett. 47, e2020GL088051 https://doi.org/10.1029/2020GL088051.

Dickson, A.G., Riley, J.P., 1979. The estimation of acid dissociation constants in sea-water media from potentiometric titrations with strong base. II. The dissociation of phosphoric acid. Mar. Chem. 7 (2), 101–109. https://doi.org/10.1016/0304-4203(79)90002-1.

Dickson, A.G., 1990. Standard potential of the reaction: $AgCl(s) + 12H_2(g) = Ag(s) + HCl(aq)$, and the standard activity constant of the ion HSO_4^- in synthetic sea water from 273.15 to 318.15 K. J. Chem. Thermodyn. 22 (2), 113–127. https://doi.org/10.1016/0021-9614(90)90074-Z.

Dickson, A.G., Sabine, C.L., Christian, J.R., 2007. Guide to Best Practices for Ocean CO_2 Measurements, vol. 3. PICES Special Publication, p. 191.

Douglas, N.K., Byrne, R.H., 2017. Achieving accurate spectrophotometric pH measurements using unpurified meta-cresol purple. Mar. Chem. 190, 66–71. https://doi.org/10.1016/j.marchem.2017.02.004.

Dunton, K.H., Goodall, J.L., Schonberg, S.V., Grebmeier, J.M., Maidment, D.R., 2005. Multi-decadal synthesis of benthic-pelagic coupling in the western arctic: role of cross-shelf advective processes. Deep-Sea Res. II 52, 3462–3477. https://doi.org/10.1016/j.dsr2.2005.09.007.

EPA, 1993. EPA Method 353.2, Revision 2.0: Determination of Nitrate-Nitrite Nitrogen by Automated Colorimetry, pp. 0–14.

Fetterer, F., Knowles, K., Meier, W.N., Savoie, M., Windnagel, A.K., 2017. Sea Ice Index. National Snow and Ice Data Center, Boulder, Colorado, USA. https://doi.org/10.7265/N5K072F8. Version 3 [Data Set].

Freitas, F.S., Arndt, S., Hendry, K.R., Faust, J.C., Tessin, A.C., Marz, C., 2022. Benthic organic matter transformation drives pH and carbonate chemistry in Arctic marine sediments. Global Biogeochem. Cycles 36, e2021GB007187. https://doi.org/10.1029/2021GB007187.

Garneau, M.-E., Gosselin, M., Klein, B., Tremblay, J.-E., Fouilland, E., 2007. New and regenerated production during a late summer bloom in an Arctic polynya. Mar. Ecol. Prog. Ser. 345, 13–26. https://doi.org/10.3354/meps06965.

Granger, J., Prokopenko, M.G., Sigman, D.M., Mordy, C.W., Morse, Z.M., Morales, L.V., Sambrotto, R.N., Plessen, B., 2011. Coupled nitrification-denitrification in sediment of the eastern Bering Sea shelf leads to ^{15}N enrichment of fixed N in shelf waters. J. Geophys. Res. 116, C11006 https://doi.org/10.1029/2010JC006751.

Grebmeier, J.M., 1987. The Ecology of Benthic Carbon Cycling in the Northern Bering and Chukchi Seas. Ph.D. Dissertation, Institute of Marine Science, University of Alaska, Fairbanks, AK, p. 189.

Grebmeier, J.M., Feder, H.M., McRoy, C.P., 1989. Pelagic-benthic coupling on the shelf of the northern Bering and Chukchi Seas, II: benthic community structure. Mar. Ecol. Prog. Ser. 51, 253–268.

Grebmeier, J.M., Smith Jr., W.O., Conover, R.B., 1995. Biological processes on arctic continental shelves: ice-ocean-biotic interactions. Arctic Oceanogr.: Marginal Ice Zones and Continental Shelves 231–261. Washington, DC.

Grebmeier, J.M., 2012. Shifting patterns of life in the Pacific Arctic and sub-Arctic seas. Ann. Rev. Mar. Sci 4, 63–78. https://doi.org/10.1146/annurev-marine-120710-100926.

Grebmeier, J.M., Bluhm, B.A., Cooper, L.W., Danielson, S.L., Arrigo, K.R., Blanchard, A. L., Clarke, J.T., Day, R.H., Frey, K.E., Gradinger, R.R., Kedra, M., Konar, B., Kuletz, K.J., Lee, S.H., Lovvorn, J.R., Norcross, B.L., Okkonen, S.R., 2015. Ecosystem characteristic and processes facilitating persistent microbenthic biomass hotspots and associated benthivory in the Pacific Arctic. Prog. Oceanogr. 135, 92–114. https://doi.org/10.1016/j.pocean.2015.05.006.

Hall, P.O.J., Rosell, E.A., Bonaglia, S., Dale, A.W., Hylen, A., Kononets, M., Nilsson, M., Sommer, S., van de Velde, S., Viktosson, L., 2017. Influence of natural oxygenation of Baltic Proper Deep Water on benthic recycling and removal of phosphorus, nitrogen, silicon, and carbon. Front. Mar. Sci. 4, 27. https://doi.org/10.3389/fmars.2017.00027.

Hancke, K., Glud, R.N., 2004. Temperature effects on respiration and photosynthesis in three diatom-dominated benthic communities. Aquat. Microb. Ecol. 37, 265–281. https://doi.org/10.3354/ame037265.

Hammond, D.E., Cummins, K.M., McManus, J., Berelson, W.M., Smith, G., Spagnoli, F., 2004. Methods for measuring benthic nutrient flux on the California Margin: comparing shipboard core incubations to in situ lander results. Limnol Oceanogr. Methods 2, 146–159. https://doi.org/10.4319/lom.2004.2.146.

Hardison, A.K., McTigue, N.D., Gardner, W.S., Dunton, K.H., 2017. Arctic shelves as platforms for biogeochemical activity: nitrogen and carbon transformations in the Chukchi Sea, Alaska. Deep-Sea Res. II 144, 78–91. https://doi.org/10.1016/j.dsr2.2017.08.004.

Henriksen, K., Blackburn, T.H., Lomstein, B.A.A., McRoy, C.P., 1990. Rates of nitrification, distribution of nitrifying bacteria and inorganic N fluxes in northern Bering-Chukchi shelf sediments. Continent. Shelf Res. 13 (5), 629–651. https://doi.org/10.1016/0278-4343(93)90097-H.

Humphreys, M.P., Lewis, E.R., Sharp, J.D., Pierrot, D., 2022. PyCO2SYS v1.8: marine carbonate system calculations in Python. Geosci. Model Dev. (GMD) 15, 15–43. https://doi.org/10.5194/gmd-15-15-2022.

Kemnitz, N., Hammond, D.E., et al., 2022. Actinium and radium fluxes from the seabed in the northeast Pacific Basin. Mar. Chem. https://doi.org/10.1016/j.marchem.2022.104180 (in press).

Kwon, S., et al., 2022. Summer net community production in the northern Chukchi Sea: comparison between 2017 and 2020. Front. Mar. Sci. 9, 1050791 https://doi.org/10.3389/fmars.2022.1050791.

Lalande, C., Grebmeier, J.M., Hopcroft, R.R., Danielson, S.L., 2020. Annual cycle of export fluxes of biogenic matter near Hanna Shoal in the northeast Chukchi Sea. Deep-Sea Res. II 177, 104730. https://doi.org/10.1016/j.dsr2.2020.104730.

Lee, K., Kim, T.-W., Byrne, R.H., Millero, F.J., Feely, R.A., Liu, Y.-M., 2010. The universal ratio of boron to chlorinity for the North Pacific and North Atlantic oceans. Geochem. Cosmochim. Acta 74 (6), 1801–1811. https://doi.org/10.1016/j.gca.2009.12.027.

Lowry, K.E., Pickart, R.S., Mills, M.M., Brown, Z.W., van Dijken, G.L., Bates, N.R., Arrigo, K.R., 2015. The influence of winter water on phytoplankton blooms in the Chukchi Sea. Deep-Sea Res. II 118, 53–72. https://doi.org/10.1016/j.dsr2.2015.06.006.

Lueker, T.J., Dickson, A.G., Keeling, C.D., 2000. Ocean pCO_2 calculated from dissolved inorganic carbon, alkalinity, and equations for K1 and K2: validation based on laboratory measurements of CO_2 in gas and seawater at equilibrium. Mar. Chem. 115 (1–2), 110–117. https://doi.org/10.1016/S0304-4203(00)00022-0.

MacGilchrist, G.A., Naveira Garabato, A.C., Tsubouchi, T., Bacon, S., Torres-Valdes, S., Azetsu-Scott, K., 2014. The Arctic Ocean carbon sink. Deep-Sea Res. I 86, 39–55. https://doi.org/10.1016/j.dsr.2014.01.002.

Mathis, J.T., Cross, J.N., Bates, N.R., 2011. The role of ocean acidification in systemic carbonate mineral suppression in the Bering Sea. Geophys. Res. Lett. 38, L19602 https://doi.org/10.1029/2011GL048884.

Moran, S.B., Kelly, R.P., Hagstrom, K., Smith, J.N., Grebmeier, J.M., Cooper, L.W., Cota, G.F., Walsh, J.J., Bates, N.R., Hansell, D.A., Maslowski, W., Nelson, R.P., Mulsow, S., 2005. Seasonal changes in POC export flux in the Chukchi Sea and implications for water column-benthic coupling in Arctic shelves. Deep-Sea Res. II 52, 3427–3451. https://doi.org/10.1016/j.dsr2.2005.09.011.

ODaly, S.H., Danielson, S.L., Hardy, S.M., Hopcroft, R.R., Lalande, C., Stockwell, D.A., McDonnell, A.M.P., 2020. Extraordinary carbon fluxes on the shallow Pacific Arctic shelf during a remarkably warm and low sea ice period. Front. Mar. Sci. 7, 548931 https://doi.org/10.3389/fmars/2020.548931.

Omar, A.M., et al., 2007. Seasonal and interannual variability of the air-sea CO_2 flux in the Atlantic sector of the Barents Sea. Mar. Chem. 104, 203–213. https://doi.org/10.1016/j.marchem.2006.11.002.

Ouyang, Z., et al., 2020. Sea-ice loss amplifies summertime decadal CO_2 increase in the western Arctic Ocean. Nat. Clim. Change 10, 678–684. https://doi.org/10.1038/s41558-020-0784-2.

Parsons, T.R., Maita, Y., Lalli, C.M., 1984. A Manual of Chemical and Biological Methods for Seawater Analysis. Pergamon Press, pp. 25–28. https://doi.org/10.1016/C2009-0-07774-5.

Pisareva, M.N., Pickart, R.S., Spall, M.A., Nobre, C., Torres, D.J., Moore, G.W.K., Whitledge, T.E., 2015. Flow of pacific water in the western Chukchi Sea: results from the 2009 RUSALCA expedition. Deep-Sea Res. I 105, 53–73. https://doi.org/10.1016/j.dsr.2015.08.011.

Redfield, A.C., 1934. In: Daniel, R.J. (Ed.), On the Proportions of Organic Derivatives in Sea Water and Their Relation to the Composition of Plankton, James Johnstone Memorial Volume. University Press of Liverpool), Liverpool, pp. 176–192.

Semiletov, I.P., 1999. Aquatic sources of CO_2 and CH_4 in the polar regions. J. Atmos. Sci. 56 (2), 286–306. https://doi.org/10.1175/1520-0469(1999)056<0286:ASASOC>2.0.CO;2.

Souza, A.C., Kim, I., Gardner, W., Dunton, K.H., 2014. Dinitrogen, oxygen, and nutrient fluxes at the sediment-water interface and bottom water physical mixing on the eastern Chukchi Sea shelf. Deep Sea Res. II 102, 77–83. https://doi.org/10.1016/j.dsr2.2014.01.002.

Stroeve, J.C., Markus, T., Boisvert, L., Miller, J., Barrett, A., 2014. Changes in Arctic melt season and implications for sea ice loss. Geophys. Res. Lett. 41, 1216–1225. https://doi.org/10.1002/2013GL058951.

Sun, H., Gao, Z.-Y., Zhao, D.-R., Sun, X.-W., Chen, L.-Q., 2021. Spatial variability of summertime aragonite saturation states and its influencing factor in the Bering Sea. Adv. Clim. Change Res. 12 (4), 508–516. https://doi.org/10.1016/j.accre.2021.04.001.

Sundby, B., Gobeil, C., Silverberg, N., Mucci, A., 1992. The phosphorus cycle in coastal marine sediments. Limnol. Oceanogr. 37 (6), 1129–1145. https://doi.org/10.4319/lo.1992.37.6.1129.

United States Geological Survey, 2019. National water quality laboratory technical. Memorandum 2, 17, 2019.

Wang, M., Overland, J.E., 2009. A sea ice free summer Arctic within 30 years? Geophys. Res. Lett. 36, L07502 https://doi.org/10.1029/2009GL037820.

Wang, K., Zhang, H., Han, X., Qui, W., 2019. Sources and burial fluxes of sedimentary organic carbon in the northern Bering Sea and the northern Chukchi Sea in response to global warming. Sci. Total Environ. 679, 97–105. https://doi.org/10.1016/j.scitotenv.2016.04.374.

Wang, H., Lin, P., Pickart, R.S., Cross, J.N., 2021. Summer surface CO_2 dynamics on the Bering Sea and eastern Chukchi Sea shelves from 1989 to 2019. J. Geophys. Res.: Oceans 127, e2021JC017424. https://doi.org/10.1029/2021JC017424.

Woodgate, R., 2018. Increases in the Pacific inflow to the Arctic from 1990 to 2015, and insights into seasonal trends and driving mechanisms from year-round Bering Strait mooring data. Prog. Oceanogr. 160, 124–154. https://doi.org/10.1016/j.pocean.2017.12.007.

Woosley, R.J., Millero, F.J., 2020. Freshening of the western Arctic negates anthropogenic carbon uptake potential. Limnol. Oceanogr. 9999, 1–13. https://doi.org/10.1002/lno.11421.

Yamamoto-Kawai, M., McLaughlin, F.A., Carmack, E.C., Nishino, S., Shimada, K., 2016. Aragonite undersaturation in the Arctic Ocean: effects of ocean acidification and sea

ice melt. Science 326 (5956), 1098–1100. https://doi.org/10.1126/science.1174190.

Yang, D., Zhao, Y., Armstrong, R., Robinson, D., 2009. Yukon River streamflow response to seasonal snow cover changes. Hydrol. Process. 23 (1), 109–121. https://doi.org/10.1002/hyp.7216.

Yasunaka, S., et al., 2018. Arctic Ocean CO_2 uptake: an improved multiyear estimate of the air-sea CO_2 flux incorporating chlorophyll a concentrations. Biogeosciences 15 (6), 1643–1661. https://doi.org/10.5194/bg-15-1643-2018.